ELSEVIER

Contents lists available at ScienceDirect

# Materials & Design

journal homepage: www.elsevier.com/locate/matdes





# Flavonoid-containing copolymers can act as both extended-release excipients and active pharmaceutical ingredients for the treatment of diabetes

Shicui Luo<sup>a,1</sup>, Qiuqiong Yang<sup>b,1</sup>, Gareth R. Williams<sup>c</sup>, Fengyu Wang<sup>a</sup>, Yamin Jia<sup>d</sup>, Wenlin Chen<sup>b,e</sup>, Huanhuan Zhao<sup>a</sup>, Liying Huang<sup>b</sup>, Anhua Shi<sup>a,b</sup>, Renjie Chang<sup>b,f,\*</sup>, Junzi Wu<sup>a,b,\*</sup>

- <sup>a</sup> Key Laboratory of Microcosmic Syndrome Differentiation, Yunnan University of Chinese Medicine, Kunming 650500, China
- b Yunnan Key Laboratory of Integrated Traditional Chinese and Western Medicine for Chronic Disease in Prevention and Treatment, Yunnan University of Chinese Medicine, Kunming 650500, China
- <sup>c</sup> UCL School of Pharmacy, University College London, 29-39 Brunswick Square, London WC1N 1AX, UK
- <sup>d</sup> College of Water Resources Science and Engineering, Taiyuan University of Technology, Taiyuan 030024, China
- e Department of Geratology, The First Affiliated Hospital of Yunnan University of Chinese Medicine, Kunming 650021, China
- f Center of Digestive Endoscopy, The First Affiliated Hospital of Yunnan University of Chinese Medicine, Kunming 650021, China

#### ARTICLE INFO

#### Keywords: Flavonoids Extended-release excipients Active pharmaceutical ingredients Diabetes Nanoparticles

#### ABSTRACT

This study focuses on multifaceted applications of plant-based natural products in the treatment of diabetes, specifically aiming to use flavonoids as both active ingredients and extended-release excipients for drug delivery. Three flavonoids (Chrysin, Biochanin A and Gardenin B) were acrylated and subsequently block copolymerised with 3-acrylamido phenyl boronic acid (AAPBA) to yield p(AAPBA-b-Chrysin), p(AAPBA-b-BiochaninA) and p (AAPBA-b-Gardenin B), collectively referred to as p(AAPBA-b-acrylic acid flavone) nanoparticles (NPs). The polymers were next formulated into NPs, and their stability, pH-responsiveness and glucose sensitivity were evaluated. These NPs can be loaded with insulin and have sustained-release properties, with insulin release being accelerated in the presence of glucose. The cytocompatibility of p(AAPBA-b-acrylic acid flavone) NPs was confirmed via cytotoxicity tests *in vitro*, which revealed that they were mainly accumulated in the liver and kidneys 24 h after injection. In a diabetic mouse model, these NPs were shown to reduce blood sugar levels in the long term; protect liver, kidney and heart function; reduce inflammatory factor levels; and balance oxidative capacity. Therefore, our flavonoid-based NPs can serve as efficient drug delivery systems for the treatment of diabetes.

#### 1. Introduction

Natural compounds have shown many advantages in the medical field as they are widely available from plant resources, have good biocompatibility and biodegradability and are highly tolerated by the body [1,2]. Many biomedical materials derived from natural products gradually decompose and are metabolised in the body, reducing potential risks caused by long-term retention [3]. However, further research is needed into the development of these materials [4,5], particularly in terms of exploring their use as multifunctional platforms.

For example, some studies have investigated the application of polysaccharides from *Bletilla striata* as excipients in the treatment of skin diseases [6,7] and also explored cell wall polysaccharides from *Panax notoginseng* [8] and other plants [9,10]. However, only a few studies have directly investigated whether natural products can be used as both active pharmaceutical ingredients and sustained-release excipients.

Flavonoids are an important group of plant extracts. They are widely found in various plants and, as monomers, exhibit significant pharmacological activity [11]. As natural anti-inflammatory and antioxidant agents, flavonoids offer various health benefits, including immunity

E-mail addresses: 303184827@qq.com (R. Chang), xnfz@ynucm.edu.cn (J. Wu).

<sup>\*</sup> Corresponding authors at: Yunnan Key Laboratory of Integrated Traditional Chinese and Western Medicine for Chronic Disease in Prevention and Treatment, Yunnan University of Chinese Medicine, Kunming 650500, China.

<sup>&</sup>lt;sup>1</sup> Authors contributed equally to this work.

enhancement, anti-diabetic effects, oxidative stress reduction and antiageing properties. Additionally, they can promote wound healing and improve microcirculation [12]. Structurally, all flavonoids share a diphenylchromone core, with different compounds arising from the various functional groups attached to it [13].

Previously [14], we showed that *p*-hydroxyphenethyl anisate could be esterified with acryloyl chloride and copolymerised to produce nanoparticles (NPs). These NPs were then loaded with insulin and tested for their potential in diabetes treatment in a murine model. The results showed that they were capable of reducing blood glucose levels, with *p*-hydroxyphenethyl anisate also exhibiting protective effects on the kidneys. We also adopted a similar approach to prepare poly(3-acrylamidophenyl boric acid-*b*-pterostilbene) NPs loaded with insulin and again observed promising physiological activity in an *in vivo* model [15]. Herein, we further explore the use of natural products as both active pharmaceutical ingredients and slow-release excipients.

First, we screened the current traditional Chinese medicine database (TCM Database@Taiwan) and selected three beneficial natural compounds: chrysin, biochanin A and gardenin B. These three flavonoids have demonstrated pronounced protective effects on the liver, kidney and heart as well as notable abilities to ameliorate oxidative stress and reduce micro-inflammatory reactions [16–18]. If acrylated, they could potentially be used to generate slow-release excipient polymers with the same pharmacological activity. To test this hypothesis, we aimed to polymerise the three flavonoids via 3-acrylamide phenylboronic acid (AAPBA) based on our previous study [14]. We here provide a full characterisation of the tested materials and explore their activity both *in vitro* and *in vivo*. Detailed experimental procedures, materials information and characterisation methods, all supported by schematic diagrams and verification data (Figs. S1–S5), are described in the Materials and methods section of the Supplementary materials.

## 2. Results and discussion

The first step of this study was to identify the optimum ratio of flavonoid to AAPBA for polymer synthesis. In the early stages, following a systematic series of trial experiments, the optimal ratio was determined based on comprehensive performance indicators such as particle size and the polydispersity index (PDI) (Fig. S6). A flavonoid-to-AAPBA ratio of 10:1 was ultimately selected.

Successful synthesis of the p(AAPBA-*b*-acrylic acid flavone) polymers was first verified via <sup>1</sup>H NMR (Fig. 1A–D and S7A–D). Fig. 1A shows the characteristic NH peak of AAPBA at 6.47 ppm (1H, 3-H). This peak shifted to 2.31 ppm (1H, 1-H) after polymerisation (Fig. 1B), indicating a significant change in the chemical environment. Additionally, as shown in parts A and B of Fig. 1, the hydrogen peaks on the C=C double bonds located at 5.75 ppm (2H, 1-H) and 6.67 ppm (1H, 2-H) moved to 2.21 ppm (1H, 3-H) and 2.75 ppm (2H, 4-H), respectively, after polymerisation. This demonstrates the breakage of C=C bonds and participation in the polymerisation reaction to generate p(AAPBA). As shown in Fig. 1B, the B-OH hydrogen peak was at 8.4 ppm (2H, 4-H), further confirming the polymerisation of p(AAPBA).

With regard to the polymerisation of p(AAPBA-*b*-chrysin), the hydrogen on the acrylic acid-chrysin C=C group moved from 6.1–6.4 ppm (1H, 2-H) and 6.6 ppm (1H, 3H) (Fig. 1C) to 2.7 ppm (1H, 2-H) and 2.4 ppm (4H, 3H) (Fig. 1D), respectively, indicating a successful reaction. In the polymerisation of p(AAPBA-*b*-Biochanin A), the original methyl hydrogen signal shifted from 3.81 ppm (1H, 1-H) to 3.95 ppm (3H, 2-H) (Fig. S7A-B). The B-OH peak was visible at 8.76 ppm (2H, 1-H) in this polymer. The hydrogen atoms on the C=C bonds also moved from 6.21 ppm (2H, 3-H) and 6.24 ppm (2H, 4-H) to 2.95 ppm (1H, 4-H), further confirming the successful polymerisation of p(AAPBA-*b*-Biochanin A). Finally, in the polymerisation of p(AAPBA-*b*-Gardenin B), the original methyl proton peak of acrylic acid-Gardenin B shifted from 3.95 ppm (9H, 1-H) to 3.56 ppm (9H, 1-H) (Fig. S7C-D). Simultaneously, the BOH proton peak also shifted from 8.4 ppm to 7.92 ppm

(1H, 3-H). The hydrogen atoms on the C=C bonds also moved from 6.45 ppm (2H, 4-H) and 6.06 ppm (2H, 5-H) to 2.91 ppm (1H, 4-H). These shifts, which denoted significant changes in the chemical environment of hydrogen atoms, also indicated successful p(AAPBA-*b*-Gardenin B) polymerisation.

Fig. S8 illustrates the <sup>13</sup>C NMR spectra obtained from the p(AAPBA-*b*-acrylic acid flavone) polymers. The carbonyl and amide groups in the polymers were difficult to observe, and only the methyl peak could be observed in the spectra. The spectra were also noisy due to the polymers' poor solubility, which meant polymer synthesis could be confirmed only via proton NMR [19].

Next, polymer synthesis was verified using infrared spectroscopy (Fig. 1E). The characteristic peaks of AAPBA included the C=O stretch (1668 cm<sup>-1</sup>), C=C stretch (1586 cm<sup>-1</sup>) and O-B-O bend (1351 cm<sup>-1</sup>). For chrysin, biochanin A and gardenin B, the characteristic peaks of diphenyl chromone included the C-O-C stretching (ca. 1164 cm<sup>-1</sup>), C=O stretching (1612–1620 cm<sup>-1</sup>) and C=O stretching (1750–1755 cm<sup>-1</sup>) of the ether bond as well as the C=C double bond stretching (1650–1655 cm<sup>-1</sup>). In the spectrum of pAAPBA, the characteristic peak of the AAPBA C=C group disappeared. For p(AAPBA-*b*-Chrysin), p(AAPBA-*b*-Biochanin A), and p(AAPBA-*b*-Gardenin B), the characteristic C=C bands also disappeared. The characteristic peaks of pAAPBA were present in all three polymers. These observations, which are in line with the findings of Sun et al. [20], indicated the successful synthesis of the three flavonoid-containing polymers.

Fig. 1F and G depict the TG and DTG profiles of pAAPBA, p(AAPBA-b-Chrysin), p(AAPBA-b-Biochanin A) and p(AAPBA-b-Gardenin B). The mass loss of pAAPBA at 50 °C–110 °C (peak at 73 °C) was due to water volatilisation. The subsequent mass losses at 218 °C and 398 °C were due to the thermal decomposition of the suspended sugar residue and that of the main chain, respectively. The residual masses of p(AAPBA-b-Chrysin) and p(AAPBA-b-Biochanin A) at 372 °C and 373 °C were similar to that of pAAPBA, and the corresponding mass losses at 434 °C and 412 °C were due to degradation of the main chain. p(AAPBA-b-Gardenin B) showed mass losses at 438 °C, also due chain degradation.

As shown in the GPC results in Fig. 2A, the Mw values of p(AAPBA-*b*-Chrysin), p(AAPBA-*b*-Biochanin A), and p(AAPBA-*b*-Gardenin B) were  $8.1 \times 10^4$ ,  $7.5 \times 10^4$  and  $8.2 \times 10^4$  Da, respectively, while the Mn values were  $7.0 \times 10^4$ ,  $6.3 \times 10^4$  and  $7.0 \times 10^4$  Da, respectively. The PDI values of these three polymers were 1.157, 1.190 and 1.171, indicating a relatively broad molecular weight distribution.

The polymers were subsequently processed into NPs, and the ζ potential of the obtained polymer-based NP formulations was initially examined (Fig. 2B). Values ranging from +10 to -10 mV commonly signify poor stability, leading to aggregation, whereas values exceeding +30 mV or below -30 mV indicate stable dispersion [21,22]. The  $\zeta$ potential values of p(AAPBA-b-Chrysin), p(AAPBA-b-Biochanin A), and p(AAPBA-b-Gardenin B) NPs were all less than -30 mV, which was indicative of their robust dispersion and stability. Analysis via dynamic light scattering (DLS) showed that these NPs had average hydrodynamic diameters of 120.3  $\pm$  0.1, 123.2  $\pm$  0.3 and 124.3  $\pm$  0.10 nm, respectively, demonstrating a uniform size profile (Fig. 2C). Further investigation of their long-term storage stability demonstrated that the NP diameters remained constant after storage at 4 °C for 40 days (Fig. 2D). It is noteworthy that the p(AAPBA-b-Chrysin) NPs were smaller than the NPs obtained from the other two compounds. This difference in size may have resulted from specific interactions between chrysin and the polymer matrix, possibly due to differences in molecular weight, hydrophobicity or steric factors affecting the self-assembly process. Subsequently, the NPs' glucose sensitivity was evaluated (Fig. 2E and F). It has been shown that at low glucose concentrations (≤1 mg/mL), preferential complexation occurs between PBA and the glucose molecule 1,2-diol, leading to cross-linking and shrinkage of PBA-based NPs [23]. Conversely, at higher glucose concentrations (>1 mg/mL), PBA-based NPs swell, resulting in a considerable increase in particle size [24]. Our results are consistent with the above observations: at pH = 7.4 and

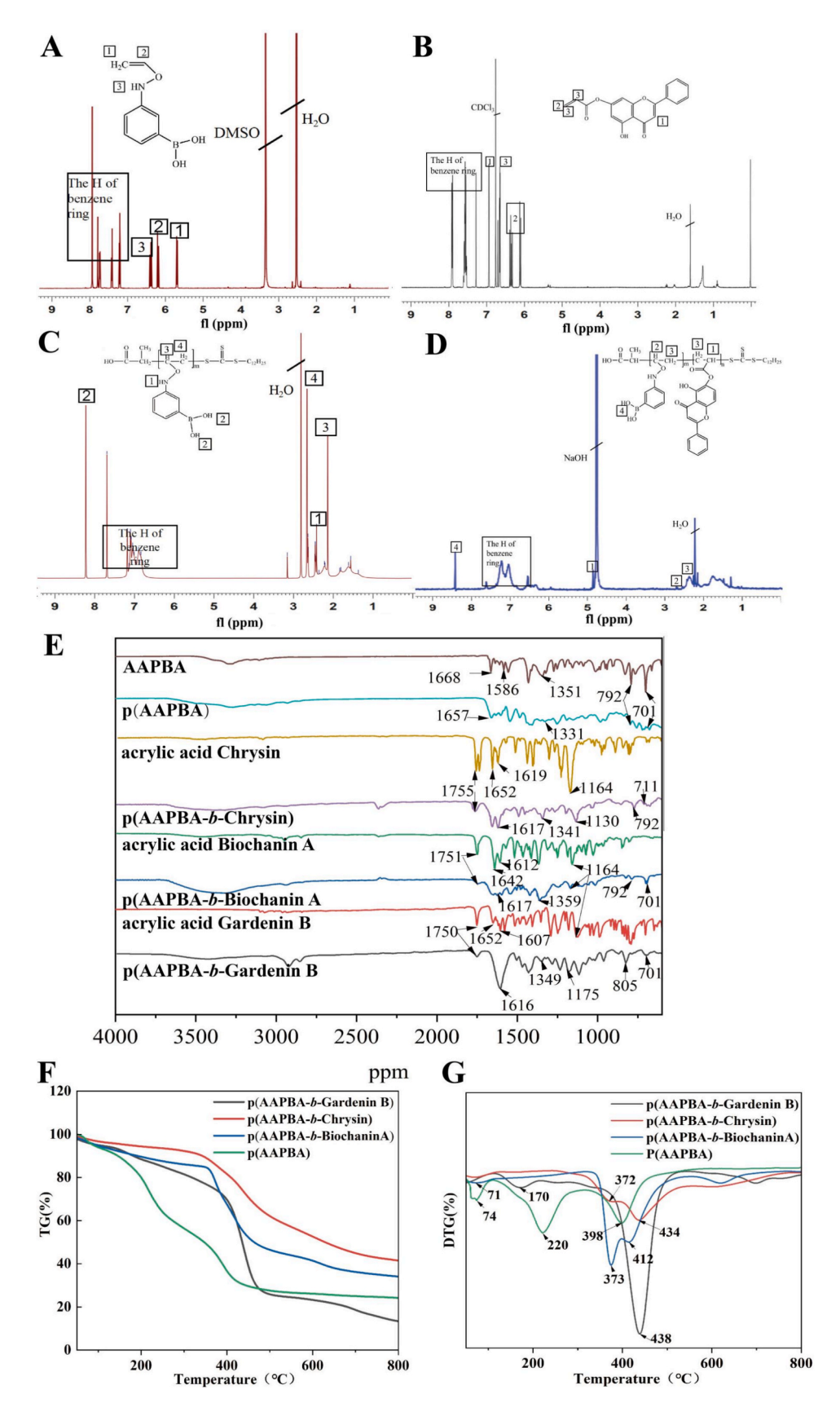
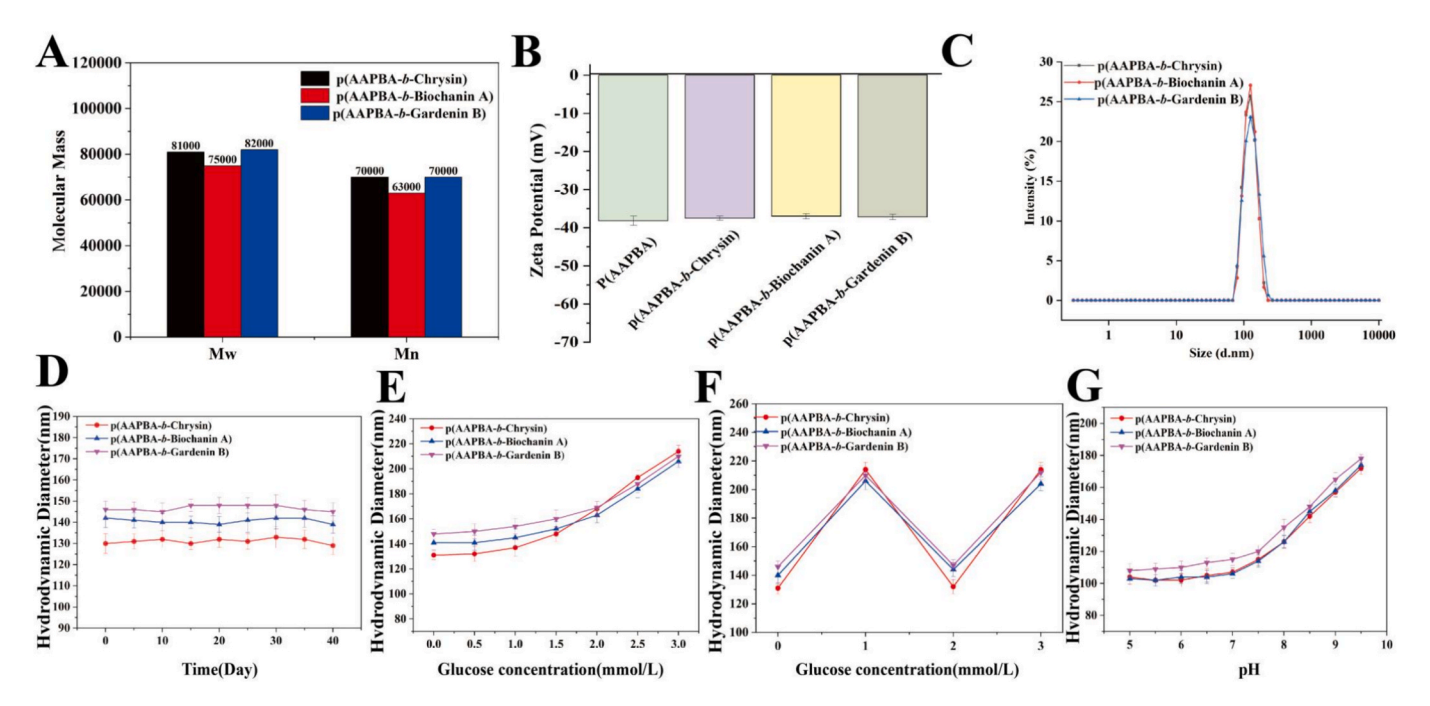


Fig. 1. Characterisation of p(AAPBA-b-acrylic acid flavone) polymers showing the <sup>1</sup>H NMR spectra of 3-acrylamidophenylboronic acid (AAPBA) (A), p(AAPBA) (B), acrylic acid-Chrysin (C), and p(AAPBA-b-Chrysin) (D), together with FTIR spectra (E). TG and DTG traces are also included in parts (F) and (G), respectively.

Materials & Design 258 (2025) 114673



**Fig. 2.** Characterisation of the p(AAPBA-*b*-acrylic acid flavone) NPs. Polymer molecular weight (A) and ζ potential values (B); distribution of NP sizes for p(AAPBA-*b*-Chrysin), p(AAPBA-*b*-Biochanin A), and p(AAPBA-*b*-Gardenin B) NPs (C); NP stability in PBS at pH 7.4 over a period of 40 days (D); hydrodynamic NP diameters in PBS supplemented with different glucose concentrations (E); measurement of the glucose elasticity of NPs (F); NP sizes in PBS at different pH levels (G).

low glucose concentrations (0–1 mg/mL), the particle sizes of p(AAPBA-b-Chrysin), p(AAPBA-b-Biochanin A), and p(AAPBA-b-Gardenin B) NPs exhibited minimal variation (Fig. 2G). However, as glucose concentration increased from 1 to 3 mg/mL, they increased by  $\sim$ 80, 60 and 55 nm, respectively. The flavonoid-containing NPs are hence glucose sensitive. Additionally, a glucose elasticity test (Fig. 2F) was conducted by assessing the NPs' response to the addition and removal of glucose. The results showed that NP size was glucose-dependent.

There has been considerable research interest into glucose-responsive drug-loaded micelles featuring PBA owing to their biocompatibility and cost-effectiveness [25,26]. However, PBA and its derivatives have an obvious disadvantage: they are pH-responsive only within a narrow range. Copolymerisation with other monomers can mitigate this problem and enhance pH-responsiveness [27]. Hence, we sought to determine whether the three flavonoids examined influenced the pH-responsiveness of the corresponding copolymers. First, the size of NPs at different pH levels was assessed (Fig. 2G). Minimal alteration was observed at pH < 7.0, whereas notable increases were observed at pH > 7.0, with particle size increasing by  $\sim\!65\text{--}70$  nm at pH 9.5. These observations indicated that the copolymer-based NPs exhibited a markedly greater pH-responsiveness compared to AAPBA, in line with previous reports [28,29].

The next step after determining the pH- and glucose-responsiveness of the polymer-based NPs was to examine their characteristics in terms of drug loading and release. As shown in detail in Tables S1–3, a suitable balance between drug loading capacity (LC%) and encapsulation efficiency (EE%) was achieved by combining 10 mg of p(AAPBA-b-Chrysin), p(AAPBA-b-Biochanin A) or p(AAPBA-b-Gardenin B) with 1 mg of insulin. The application of lower glucose concentrations led to a higher EE% but lower LC%, whereas higher concentrations resulted in a higher LC% but reduced EE%. At a polymer: insulin w/w ratio of 10:1, the LC% was ca. 7.4 %–7.8 %, with an EE% ranging between 70 % and 78 %. This LC% was lower than that obtained for p(AAPBA-b-N-vinylcaprolactam) [30] and p(AAPBA-b-diethylene glycol methyl ether methacrylate) [31] NPs synthesised in our previous research. This discrepancy may be due to the low hydrophilicity of flavones compared to N-vinylcaprolactam or diethylene glycol methyl ether methacrylate. Subsequent analysis of the

morphology of NPs after insulin encapsulation (Fig. 3A–C) revealed that they retained their spherical shape but increased in size, and NP aggregation was observed in TEM images. When comparing DLS and TEM images, the NPs appeared smaller in the latter than in the former.

After storage at 4 °C, 25 °C and 37 °C in PBS for 20 days, the diameter of the insulin-loaded NPs was found to be largely unchanged (Fig. S9A–C). With regard to the particles' pH-responsiveness (Fig. S9D–F), a notable growth in size was observed at pH > 7.5.

Generally, insulin-loaded NPs are designed to ensure controlled release, i.e. they allow the gradual release of insulin in response to increasing glucose concentrations. The biological activity of insulin depends on its secondary and tertiary structures, and if such structures are degraded during encapsulation or release, its function will be affected. In this study, circular dichroism spectroscopy was used to assess the structural integrity of insulin after release. As depicted in Fig. S10, fresh insulin exhibited characteristic peaks at 208 nm and 222 nm in the near-ultraviolet region, corresponding to the  $\alpha$ -helical structure and  $\beta$ -pleated sheets, respectively. These peaks were also detected in the insulin released from the NPs, suggesting minimal alteration in structure. Analysis of FTIR spectra (Fig. S11A) showed that insulin had an amide II signal peak near 1550 cm<sup>-1</sup>. Compared with the polymer thermogravimetric graph (Fig. 1F and G), the TGA results (Fig. S11B, C) indicated that the insulin-loaded NPs exhibited higher thermal decomposition and main chain degradation temperatures, better thermal stability and a slightly higher residual mass.

In subsequent experiments, insulin release was investigated at glucose concentrations of 0 mg/mL and 3 mg/mL. As shown in Fig. 3E and 4F, the release profiles of insulin-loaded p(AAPBA-b-Chrysin) and insulin-loaded p(AAPBA-b-Biochanin A) NPs were very similar, whereas the profile of insulin-loaded p(AAPBA-b-Gardenin B) NPs, while still similar to those above, was less so, showing a greater extent of release at each timepoint. At 0 mg/mL glucose, drug release occurred over a period of 24 h, whereas at 3 mg/mL glucose, release was accelerated and completed after 12 h. The AAPBA group in the insulin-loaded p(AAPBA-b-Chrysin), p(AAPBA-b-Biochanin A) and p(AAPBA-b-Gardenin B) NPs is thought to play a key role in regulating drug release. This group can specifically bind to the dihydroxyl group in glucose to form a

Materials & Design 258 (2025) 114673

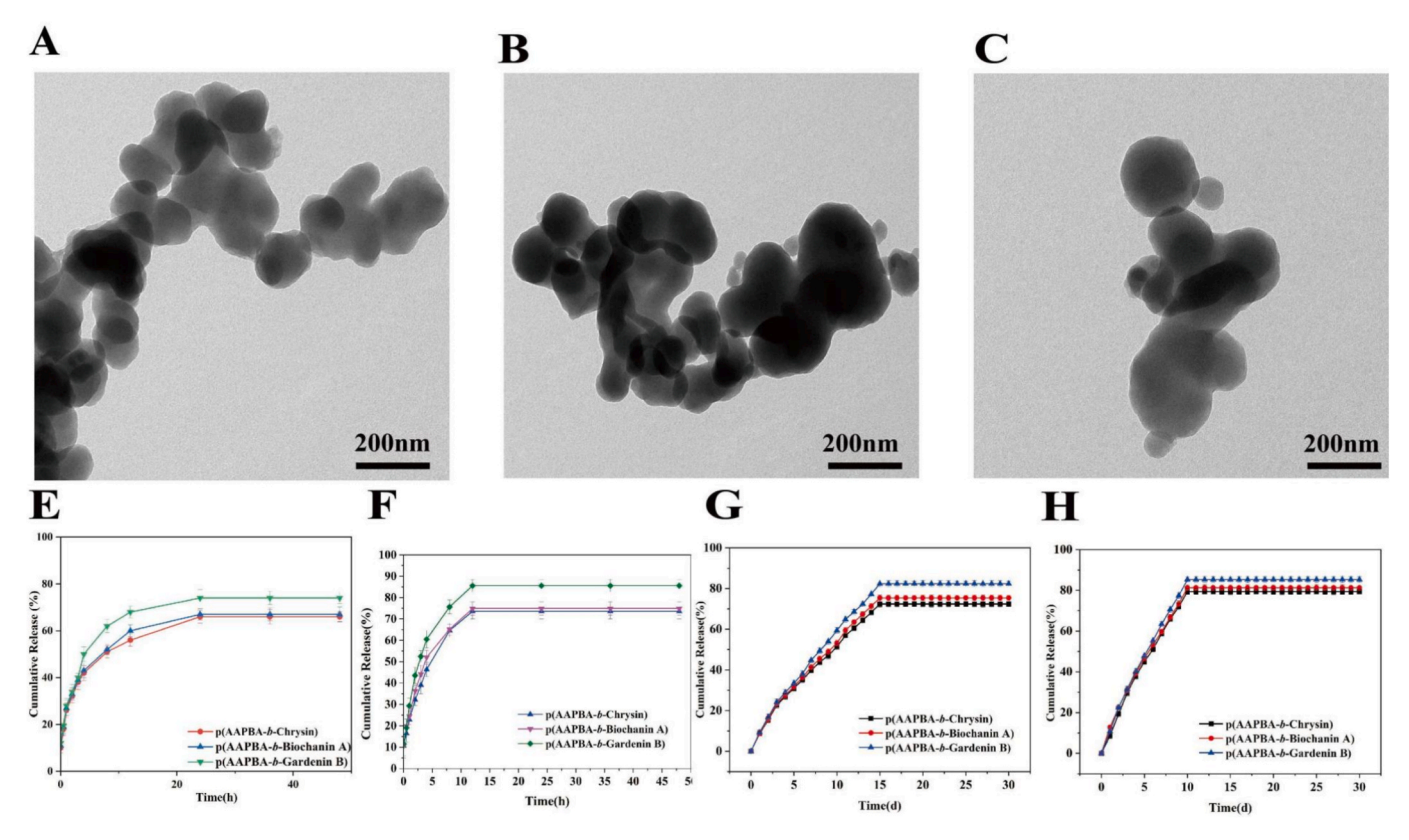


Fig. 3. Drug loading and release from p(AAPBA-*b*-Acrylic acid flavone) NPs. TEM images of insulin-loaded p(AAPBA-*b*-Chrysin) (A), p(AAPBA-*b*-Biochanin A) (B), and p(AAPBA-*b*-Gardenin B) (C) NPs; cumulative insulin release *in vitro* at glucose concentrations of 0 mg/mL (E) and 3 mg/mL (F); cumulative flavone release *in vitro* at glucose concentrations of 0 mg/mL (G) and 3 mg/mL (H).

hydrophilic borate structure. As glucose concentration increases, the binding force between the AAPBA group and glucose also increases, causing the originally hydrophobic polymer to gradually transform into a hydrophilic compound. This structural transformation leads to significant changes in the size and glucose sensitivity of NPs [32], accelerating the insulin release process. The reduced release observed for p (AAPBA-b-Chrysin) and p(AAPBA-b-Biochanin A) NPs compared to p (AAPBA-b-Gardenin B) NPs could be attributed to hydroxyl groups in chrysin and biochanin A facilitating the formation of stable complexes with insulin.

Flavonoid release occurred over a period of ca. 10–16 days and then reached a plateau (Fig. 3G-H). No marked differences were observed between the insulin-loaded p(AAPBA-*b*-Chrysin) and p(AAPBA-*b*-Biochanin A) NPs, whereas p(AAPBA-*b*-Gardenin B) again showed a slightly more rapid release. Release varied under different glucose concentrations, occurring over 16 days and 10 days at glucose concentrations of 0 mg/mL (Fig. 3G) and 3 mg/mL (Fig. 3H), respectively.

Flavonoids exhibit specific pharmacological activities [33]; however, the impact on such activities after flavonoid incorporation into polymers remains uncertain. To address this question, L02 and HepG2 cells were used to investigate the cytocompatibility of the flavonoid-containing NPs (Fig. 4A and B). The relative viability of healthy L02 cells exceeded 80 % after 24 h of incubation with the NPs; the same as that of untreated cells or even greater. Conversely, some toxicity was detected for HepG2 cells, with viability below 80 % after 24 h of incubation in some cases. This indicated that the NPs are slightly toxic to cancer cells, in accordance with the known antitumor effects of flavonoids [341].

Subsequently, the NPs' safety was further evaluated *in vivo* through both short-term high-dose and long-term low-dose administration in mice. By providing information on accumulated toxicity, long-term exposure to low doses assists in elucidating chronic harm [35]. Mice

received daily subcutaneous injections at a low dosage of 20 mg/kg for 60 days. Subsequent routine blood tests were conducted to examine the number and morphology of various blood cells. As illustrated in Fig. 4C and Table S4, none of the measured indicators in the experimental groups differed significantly from those in the control (p > 0.05). H&E staining demonstrated no apparent damage to the liver, kidney, heart, spleen and lung tissues of mice, confirming the NPs' non-toxicity (Fig. 4D). Moreover, no pathological changes were observed in the mice's skin on the 60th day post-injection (Fig. 4E). Specifically, the skin of mice in the p(AAPBA-b-Chrysin), p(AAPBA-b-Biochanin A) and p (AAPBA-b-Gardenin B) NP-treated groups showed no obvious signs of pigmentation, ulceration or inflammation compared with the control group. At the same time, histological sections showed that the epidermis and dermis of mice in each group were intact, with no obvious signs of inflammatory cell infiltration or fibrosis, further proving that these NPs do not cause skin damage under long-term exposure. After testing chronic toxicity, we then investigated acute toxicity. Detailed results are provided in Figs. S12 and S13 and Table S5. No toxicity was observed in this case either.

The biodistribution and metabolism of our NP formulations were explored following subcutaneous injection into the back of mice. Fluorescence images revealed that fluorescence in the free DiR group was visible in every part of the body at  $12\ h$  after injection and completely disappeared after  $72\ h$ . Conversely, fluorescence in the NP-treated groups was concentrated at the injection site (extending towards the side) at  $12\ h$  and lasted for  $84–96\ h$  (Figs. S14A, S15), indicating that the NPs persisted in the body for a prolonged period of time. Most previous reports [36,37] indicate that DiR has a fluorescence quenching time of  $24–48\ h$ , whereas in this study it was  $72–96\ h$ .

Experiments testing NP distribution in different organs (Fig. S14B-C) showed that the DiR group mainly accumulated in the liver after 24 h (intensity order: liver > kidney > lung > spleen > heart), whereas NPs

Materials & Design 258 (2025) 114673

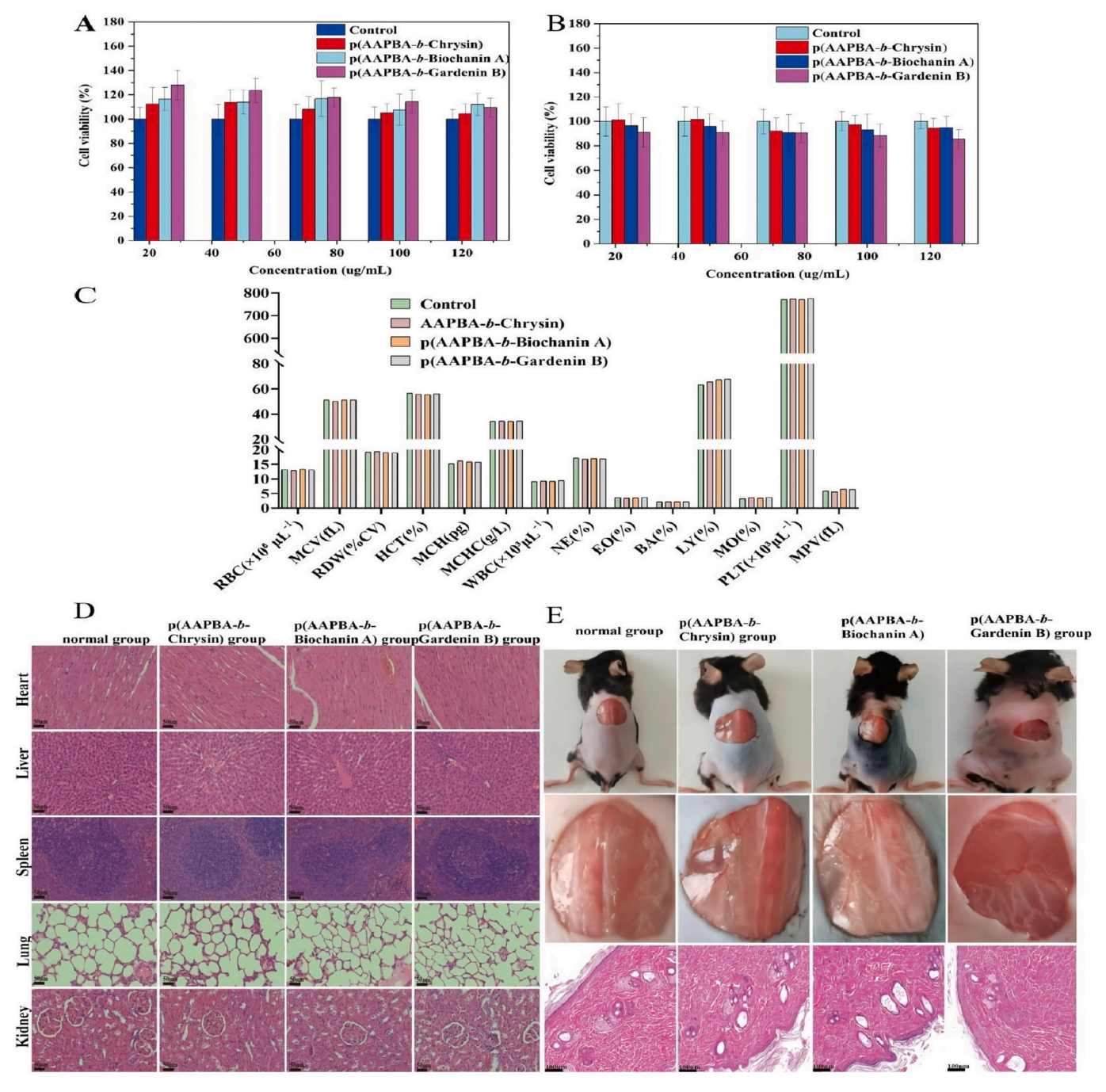


Fig. 4. Cytocompatibility and *in vivo* chronic toxicity of p(AAPBA-b-acrylic acid flavone) NPs. Cytocompatibility was tested on healthy L02 (A) and cancerous HepG2 (B) cells. (C) Histogram showing key blood biochemical markers after 60 days of treatment; (D) H&E staining images of the heart, liver, spleen, lung and kidney (scale bar = 50  $\mu$ m); (E) photos of the injection site and representative H&E images of the skin of mice (scale bar = 50  $\mu$ m) (E).

were concentrated in the liver and kidney. The high fluorescence in the liver may be related to the specific binding of the B-OH group of AAPBA in the NPs to the sialic acid on the liver surface. This result reveals the liver-targeting ability of the NP formulations as well as their advantages in terms of sustained release, providing an important reference for the design of drug delivery systems.

To establish the effect of the NP formulations, free insulin, blank NPs and insulin-loaded NPs were set as control groups. Due to restrictions on the number of animals posed by ethical guidelines for animal experimentation, this study only tested cellular inflammatory factors and oxidative stress indicators in the three control groups, and the results showed good biosafety levels (Fig. S16). Additionally, further experiments were conducted on the anti-inflammatory effects of chrysin,

chickpea protein A, gardenia protein B and their polymers on RAW 264.7 macrophages stimulated by lipopolysaccharides. Experimental data showed that the three flavonoid compounds still retained significant pharmacological activity after polymerisation (Fig. S17).

The *in vivo* hypoglycaemic effects of the NP formulations were next evaluated (Fig. 5A-B). The control (healthy mice given a normal diet) and diabetic groups exhibited stable blood glucose levels, maintained at 6 mmol/L in the former and at 24 mmol/L in the latter. Blood glucose levels in the three NP-treated groups dropped rapidly within the first few hours after injection, as similarly observed in the insulin injection group. However, a significantly greater amount of time was required for blood glucose levels to rise again in the NP-treated groups than in the insulin injection group. The NP formulations clearly have a significant

S. Luo et al. Materials & Design 258 (2025) 114673

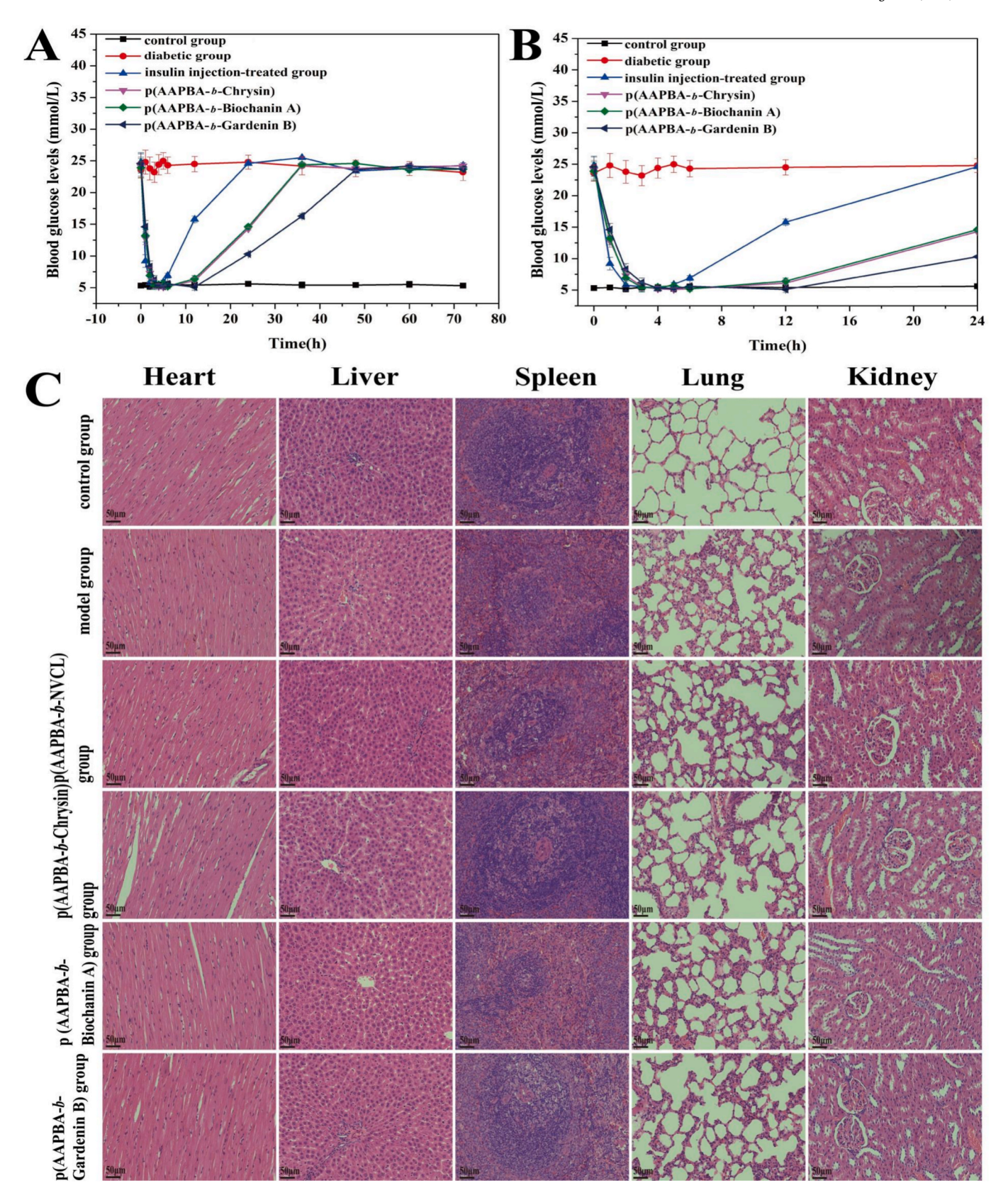


Fig. 5. Changes in blood glucose concentration in mice given various p(AAPBA-*b*-flavone)-based treatments, measured over 72 h (A) and 24 h (B); (C) H&E images of the heart, liver, spleen, lung and kidney tissues of mice after 4 weeks of treatment with NPs (scale bar = 50 µm).

hypoglycaemic effect and maintain a lower blood sugar level. These results suggested that insulin-loaded NPs effectively lower blood glucose levels over a period of 24 h after injection.

Further tests were then conducted on the pharmacological effects of the flavonoids contained in the NP formulations. To do so accurately, we used the insulin-loaded p(AAPBA-b-NVCL) NPs synthesised in our previous study as a control [38]. As shown in the histopathological images included in Fig. 5C, the control group's heart, liver, spleen, lung and kidney tissues exhibited no abnormalities, whereas the diabetic group displayed significant damage in the heart, liver and kidney, as evidenced by an increased amount of diseased tissue, cell necrosis and inflammatory cell infiltration. Compared to the diabetic group, the p(AAPBA-b-NVCL) NP-treated control group and the groups treated with the flavonoid-enriched NP formulations [p(AAPBA-b-Chrysin), p(AAPBA-b-Biochanin A), and p(AAPBA-b-Gardenin B)] showed some improvement, as reflected by a reduction in both inflammatory cell infiltration and amount of necrotic tissue and a more organised tissue structure. These histological changes suggest a protective effect against diabetes-induced damage. Notably, the groups treated with the flavonoid-based NP formulations demonstrated superior therapeutic effects compared to the p (AAPBA-b-NVCL) NP-treated group. Relevant biochemical indicators—such as cTnI, SCr, UA, AST and ALT for liver, kidney and heart function, as well as T-AOC, GSH, SOD, Hs-CRP, IL- $1\alpha$ , IL-6 and TNF- $\alpha$  for inflammation and oxidative stress—were significantly improved after NP treatment (Fig. 6). At the same time, the groups treated with the flavonoid-based NP formulations showed greater improvements compared to the p(AAPBA-b-NVCL) group. This was specifically manifested by significant reductions in the levels of inflammatory markers, such as TNF- $\alpha$ , IL-1 $\alpha$  and IL-6, as well as reductions in levels of ALT and AST, indicating improved liver function. This stronger effect likely derives from the release of flavonoids from the NPs. The p(AAPBA-b-NVCL) NP-treated group also showed some improvement, possibly due to the protective effect of encapsulated insulin.

#### 3. Conclusions

This study investigated the use of naturally occurring flavonoids both as active pharmaceutical ingredients and excipients to achieve extended drug release for diabetes treatment. A nanodelivery system was successfully developed by constructing smart responsive block copolymers containing three flavonoids (chrysin, biochanin A and gardenin B) and AAPBA. This system breaks through the limitation of traditional carriers with only a single delivery function and achieves the synergistic effect of controlled insulin release and flavonoid active ingredients. *In vivo* experiments confirmed that compared with insulin injection alone, the injection of insulin-encapsulated polymer-based NPs prolonged the

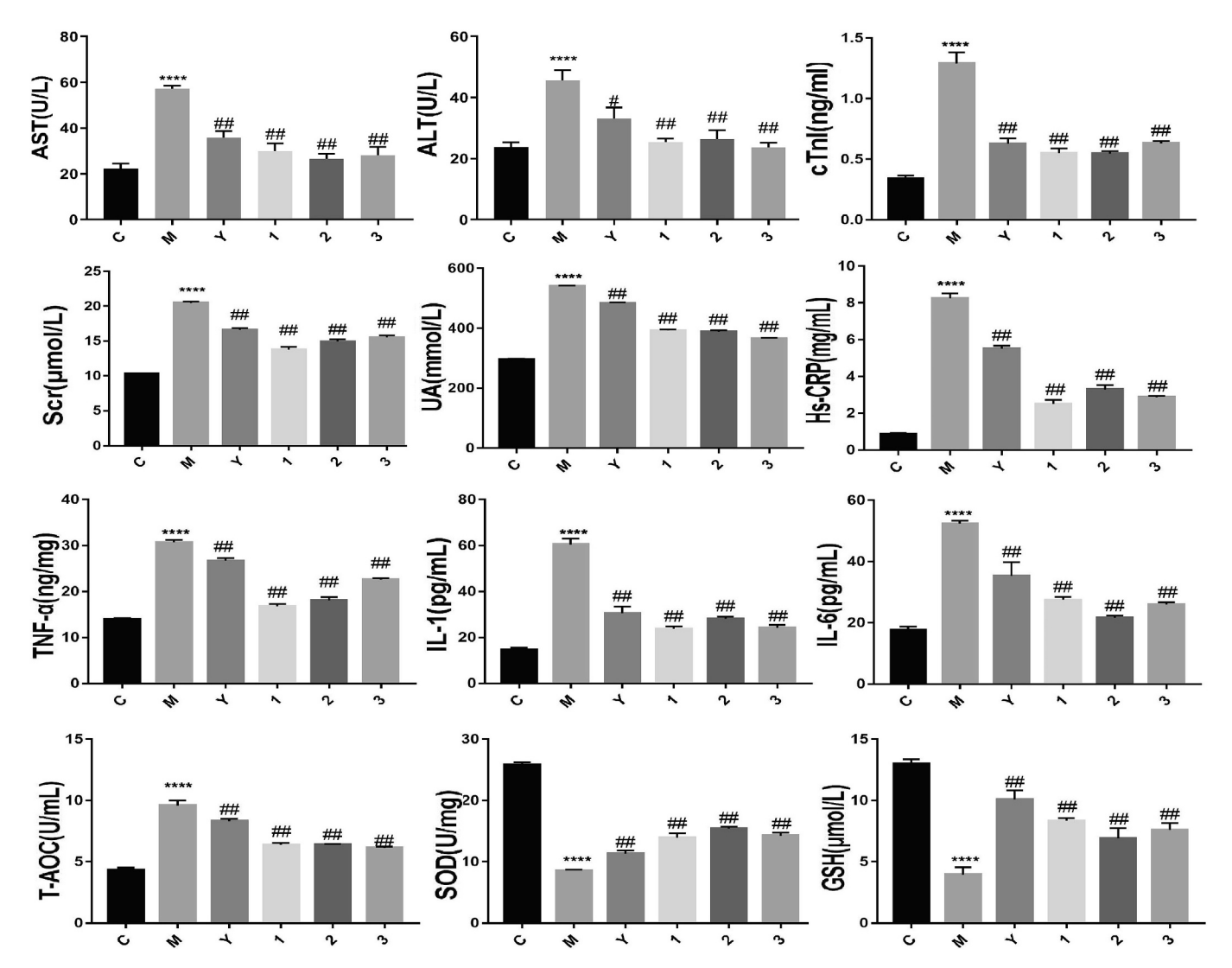


**Fig. 6.** Effect of NPs on biochemical parameters at 60 days after administration in the control group (C), diabetic model group (M), p(AAPBA-b-NVCL) group (Y), p (AAPBA-b-Chrysin) group (1), p (AAPBA-b-Biochanin A) group (2) and p(AAPBA-b-Gardenin B) group (3); \*\*\*\*\*: p < 0.01 vs control group; \*#: p < 0.05 vs control group.

blood glucose regulation time in a diabetic mouse model. Measurements of cTnI, SCr, UA, AST, ALT, T-AOC, GSH, SOD, Hs-CRP, IL-1 $\alpha$ , IL-6 and TNF- $\alpha$ , which are markers of inflammation and oxidative stress, revealed significant improvements after NP treatment.

However, this study has some limitations. The main chains of the three block copolymers are all carbon chains and not biodegradable. Although we verified the NPs' safety through relevant experiments, the excretion mechanism is still unclear. At the same time, the prepared NPs still have deficiencies in terms of particle size uniformity and dispersibility. TEM images showed a relatively large particle size and some degree of aggregation. These characteristics may have a certain impact on the stability and drug delivery effect of its subsequent *in vivo* applications. Therefore, future research should focus on optimising the NP preparation process; improving particle dispersibility and size uniformity; and further systematically evaluating *in vitro* and *in vivo* NP behaviour and sustained-release performance to promote the practical application of this nanodelivery system.

# Consent for publication

Not applicable.

#### CRediT authorship contribution statement

Shicui Luo: Writing – original draft, Investigation. Qiuqiong Yang: Investigation, Data curation. Gareth R. Williams: Writing – review & editing, Formal analysis. Fengyu Wang: Investigation, Data curation. Yamin Jia: Visualization, Methodology. Wenlin Chen: Funding acquisition. Huanhuan Zhao: Methodology, Investigation. Liying Huang: Writing – review & editing. Anhua Shi: Resources, Conceptualization. Renjie Chang: Resources, Conceptualization. Junzi Wu: Investigation, Funding acquisition, Conceptualization.

# Ethics approval and consent to participate

All experiments were approved by the Animal Use and Ethics Committee of the Yunnan University of Chinese Medicine (R062023325).

# Funding

This work acknowledges funding from the Young Scientists Fund of the National Natural Science Foundation of China (82104403) and the Open Project of Yunnan Clinical Medical Research Center for Geriatric Diseases (2023YJZX-LN08 and 2023YJZX-LN10).

## Declaration of competing interest

The authors declare that they have no known competing financial interests or personal relationships that could have appeared to influence the work reported in this paper.

# Appendix A. Supplementary data

Supplementary data to this article can be found online at https://doi. org/10.1016/j.matdes.2025.114673.

### Data availability

Data will be made available on request.

#### References

- [1] Y. Dai, K. Qiao, D. Li, et al., Plant-derived biomaterials and their potential in cardiac tissue repair, Adv. Healthc. Mater. 12 (20) (2023) 2202827.
- [2] S. Ai, Y. Li, H. Zheng, et al., Collision of herbal medicine and nanotechnology: A bibliometric analysis of herbal nanoparticles from 2004 to 2023, J. Nanobiotechnol. 22 (1) (2024) 140.

- [3] E. Oledzka, Xanthohumol—a miracle molecule with biological activities: A review of biodegradable polymeric carriers and naturally derived compounds for its delivery, Int. J. Mol. Sci. 25 (6) (2024) 3398.
- [4] J.B. Reolon, M.H.M. Sari, C. Marchiori, et al., Herbal drugs-loaded soft nanoparticles for treating skin disorders: Where do we stand? Ind. Crop. Prod. 206 (2023) 117602.
- [5] Z. Xu, M. Dong, S. Yin, et al., Why traditional herbal medicine promotes wound healing: Research from immune response, wound microbiome to controlled delivery, Adv. Drug Deliv. Rev. 195 (2023) 114764.
- [6] K. Gou, Y. Li, Y. Qu, et al., Advances and prospects of Bletilla striata polysaccharide as promising multifunctional biomedical materials, Mater. Des. 223 (2022) 111198
- [7] X.D. Shi, J.Y. Yin, S.W. Cui, et al., Plant-derived glucomannans: Sources, preparation methods, structural features, and biological properties, Trends Food Sci. Technol. 99 (2020) 101–116.
- [8] M.M. Ahmad, Recent trends in chemical modification and antioxidant activities of plants-based polysaccharides: A review, Carbohydr. Polym. Technol. Appl. 2 (2021) 100045.
- [9] X. Liu, C.M.G.C. Renard, S. Bureau, et al., Revisiting the contribution of ATR-FTIR spectroscopy to characterize plant cell wall polysaccharides, Carbohydr. Polym. 262 (2021) 117935.
- [10] Y. Liu, L. Wang, Extracellular vesicles targeting non-parenchymal cells: The therapeutical effect on liver fibrosis, eGastroenterology 2 (1) (2024) e100040.
- [11] J.A. Kazlauskaite, M. Marksa, J. Bernatoniene, Impact of polyvinylpyrrolidone-vinyl acetate copolymer and sodium starch glycolate excipients on phenolic extraction from red clover: Enhancing biological activity and antioxidant potential, Pharmaceutics 16 (3) (2024) 399.
- [12] G.A. Kumar, S. Kumar, R. Bhardwaj, et al., Recent advancements in multifaceted roles of flavonoids in plant–rhizomicrobiome interactions, Front. Plant Sci. 14 (2024) 1297706.
- [13] H. Tao, L. Li, Y. He, et al., Flavonoids in vegetables: Improvement of dietary flavonoids by metabolic engineering to promote health, Crit. Rev. Food Sci. Nutr. 64 (11) (2024) 3220–3234.
- [14] Q. Ma, L. Bian, X. Zhao, et al., Novel glucose-responsive nanoparticles based on p-hydroxyphenethyl anisate and 3-acrylamidophenylboronic acid reduce blood glucose and ameliorate diabetic nephropathy, Mater. Today Bio 13 (2022) 100181.
- [15] X. Zhao, A. Shi, Q. Ma, et al., Nanoparticles prepared from pterostilbene reduce blood glucose and improve diabetes complications, J. Nanobiotechnol. 19 (2021) 1–18.
- [16] A. Salama, A.H. Salama, M.H. Asfour, Tannic acid coated nanosuspension for oral delivery of chrysin intended for anti-schizophrenic effect in mice, Int. J. Pharm. 656 (2024) 124085.
- [17] H. Akit, E. Ozan, R. Erenler, Isolation, characterization, and antiproliferative activity of polymethoxy flavones from mentha dumetorum, Nat. Prod. J. 13 (7) (2023) 20–26.
- [18] S. Govindasami, V.V.S. Uddandrao, N. Raveendran, et al., Therapeutic potential of biochanin-a against isoproterenol-induced myocardial infarction in rats. cardiovascular & hematological agents in medicinal chemistry (formerly current medicinal chemistry-cardiovascular, Hematological Agents 18 (1) (2020) 31–36.
- [19] Y. Liang, P.Y. Wang, Z.Y. Liu, et al., Dual stimuli-responsive micelles for imaging-guided mitochondrion-targeted photothermal/photodynamic/chemo combination therapy-induced immunogenic cell death, Int. J. Nanomed. (2023) 4381–4402.
- [20] K. Sun, S.W.A. Bligh, H. Nie, et al., Lectin recognizing thermoresponsive double hydrophilic glycopolymer micelles by RAFT polymerization, RSC Adv. 4 (66) (2014) 34912–34921.
- [21] S. Cui, Z. Yang, D.J. McClements, et al., Stability mechanism of Pickering emulsions co-stabilized by protein nanoparticles and small molecular emulsifiers by two-step emulsification with different adding sequences: From microscopic to macroscopic scales, Food Hydrocoll. 137 (2023) 108372.
- [22] S. Cui, D.J. McClements, J. Shi, et al., Fabrication and characterization of low-fat Pickering emulsion gels stabilized by zein/phytic acid complex nanoparticles, Food Chem. 402 (2023) 134179.
- [23] S. Morariu, Advances in the design of phenylboronic acid-based glucose-sensitive hydrogels, Polymers 15 (3) (2023) 582.
- [24] J. Su, J. Qian, W. Zeng, et al., Effective adsorption of salvianolic acids with phenylboronic acid functionalized polyethyleneimine-intercalated montmorillonite, Sep. Purif. Technol. 311 (2023) 123304.
- [25] W. Jiang, M. Liang, Q. Lei, et al., Phenylboronic acid-functionalized chitosan for enabling transmucosal delivery for cancer therapy, Mater. Des. 229 (2023) 111843
- [26] M. Orságh, B. Strachota, E. Pavlova, et al., Meta-isobutoxy phenylboronic acid for nanoscale multi-stimuli-responsive low-molecular-weight hydrogelator, ACS Appl. Nano Mater. 6 (17) (2023) 16055–16064.
- [27] M. Khanal, T. Vausselin, A. Barras, et al., Phenylboronic-acid-modified nanoparticles: Potential antiviral therapeutics, ACS Appl. Mater. Interfaces 5 (23) (2013) 12488–12498.
- [28] D.M. Kim, J.M. Moon, W.C. Lee, et al., A potentiometric non-enzymatic glucose sensor using a molecularly imprinted layer bonded on a conducting polymer, Biosens. Bioelectron. 91 (2017) 276–283.
- [29] S. Liu, Y. Sun, D. Guo, et al., Porous boronate imprinted microsphere prepared based on new RAFT functioned cellulose nanocrystalline with multiple H-bonding at the emulsion droplet interface for highly specific separation of Naringin, Chem. Eng. J. 452 (2023) 139294.
- [30] J. Wu, D.H. Bremner, H. Li, et al., Synthesis and evaluation of temperature-and glucose-sensitive nanoparticles based on phenylboronic acid and Nvinylcaprolactam for insulin delivery, Mater. Sci. Eng. C 69 (2016) 1026–1035.

- [31] J.Z. Wu, G.R. Williams, H.Y. Li, et al., Glucose-and temperature-sensitive nanoparticles for insulin delivery, Int. J. Nanomed. (2017) 4037–4057.
- [32] M. Vitulo, E. Gnodi, R. Meneveri, et al., Interactions between nanoparticles and intestine, Int. J. Mol. Sci. 23 (8) (2022) 4339.
- [33] A.N. Panche, A.D. Diwan, S.R. Chandra, Flavonoids: An overview, J. Nutr. Sci. 5 (2016) e47.
- [34] A. Samanta, G. Das, S.K. Das, Roles of flavonoids in plants, Carbon 100 (6) (2011) 12–35.
- [35] C. Lasagna-Reeves, D. Gonzalez-Romero, M.A. Barria, et al., Bioaccumulation and toxicity of gold nanoparticles after repeated administration in mice, Biochem. Biophys. Res. Commun. 393 (4) (2010) 649–655.
- [36] S. Huang, T. Wen, J. Wang, et al., Nanoparticle-integrated dissolving microneedles for the co-delivery of R848/aPD-1 to synergistically reverse the immunosuppressive microenvironment of triple-negative breast cancer, Acta Biomater. 176 (2024) 344–355.
- [37] D.Y. Usta, S. Olgac, B. Timur, et al., Development and pharmacokinetic evaluation of Neusilin® US2-based S-SNEDDS tablets for bosentan: Fasted and fed states bioavailability, IVIS® real-time biodistribution, and ex-vivo imaging, Int. J. Pharm. 643 (2023) 123219.
- [38] J. Wu, Y. Yang, S. Li, et al., Glucose-sensitive nanoparticles based on poly (3-acrylamidophenylboronic acid-block-n-vinylcaprolactam) for insulin delivery, Int. J. Nanomed. (2019) 8059–8072.